CONSIDERATION OF DAMAGES OF A FLOATING ROOF-TYPE OIL STORAGE TANK DUE TO THERMAL STRESS

Yoshihiro Hirokawa[1], Minoru Yamada[1], Haruki Nishi[1],
Shinsaku Zama[1], and Ken Hatayama[1]

[1]Research and Development Division, National Research Institute of Fire and Disaster
4-35-3 Jindaiji-Higashimachi, Chofu-city, Tokyo 182-8508, Japan

Abstract
Several cracks were found on some actual floating roofs of the crude oil tanks in a southern Japan refinery. It was assumed that one of the causes is due to thermal stress during the day. In order to figure out whether the thermal stress could cause damage on the floating roof, strain and temperature were measured on the actual floating roof by using optical fiber gauges. Furthermore, thermal stress analysis and fracture possibility estimation were also carried out as additional analysis. As a result, thermal stress on the floating roof turned to be relatively small and could not cause the initial crack. However, the temperature fluctuation in a day could affect the crack propagation.

Key words: *Oil storage tank, Floating roof, Measurement, Optical fiber gauge, Thermal stress analysis, FEM, Fracture probability, Crack*

1. Introduction

An oil storage tank equipped with a floating roof is called a floating roof tank [1]. The floating roof covers the oil surface in order to prevent volatilization and contamination. The single-deck type floating roof is mainly composed of a thin deck and a pontoon maintaining buoyancy. The deck thickness does not depend on tank size and approximately 5mm thick steel plate is used even if the diameter is as much as 100m. Therefore, the floating roof is vulnerable to the external load such as earthquake motion. For example, the Tokachi-oki earthquake ground motion hit Tomakomai city in Hokkaido in Japan in 2003 and around 200 tanks had the damage in Hokaido at that time. One of them in Tomakomai city suffered serious damages on the floating roof. The roof lost the buoyancy from the pontoon and sank completely. As a result, the tank was on a whole surface fire for 44 hours [2].

According to the recent investigation conducted by the authors, several cracks were found on the floating roof of the crude oil tank in a southern Japan refinery [3]. The tank has 100,000 kL capacity, 80m diameter, and 22m height. The geographical features are that the refinery is located in the area where several big typhoons tend to pass every year and that the temperature difference between day and night is relatively large. In order to prevent the potential serious incident, it is necessary to investigate causes of the cracks on the floating roof.

In this study, it was assumed that one of the causes was due to thermal stress on the floating roof tank during the day. Strain and temperature on the floating roof were measured by using an optical fiber gauge in order to comprehend the floating roof during the day. Thermal stress analysis was also conducted by using the finite element method (FEM) in order to compare with the measurement results on the actual floating roof. In addition to that, the fracture possibility of the deck plate due to cyclic thermal stress was estimated by means of probabilistic fracture mechanics approach.

2. Measurement on the Actual Floating Roof

In order to figure out whether the thermal stress could cause damage on the floating roof, strain and temperature were measured on the actual floating roof by using optical fiber gauges. The measurements were conducted on March, June and August in 2008 and on August in 2009.

2.1 Sensor layout

The floating roof on which several cracks were found is the single-deck type floating roof with an additional center pontoon. The tank has a diameter of 80m and height of 22m with a 100,000 kL capacity. The thickness of the deck plate is 4.8mm. The tank was built in 1980.

In order to measure thermal stress amplitude during the day, optical fiber gauges equipping with the explosion-proof were adhered to the roof surface. Figure 1 and Figure 2 show the actual floating roof and layout optical fiber gauges to measure strain and temperature amplitude. “STR#” in

Table 1 shows the distance of strain gauges from the wall of the center pontoon. Temperature gauges were set in between STR2 and STR3 beside the line of the strain gauge sensor.

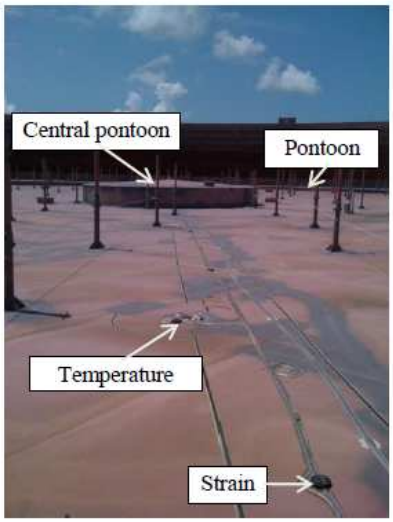

Figure 1 Actual floating roof equipped with pontoon and center pontoon.

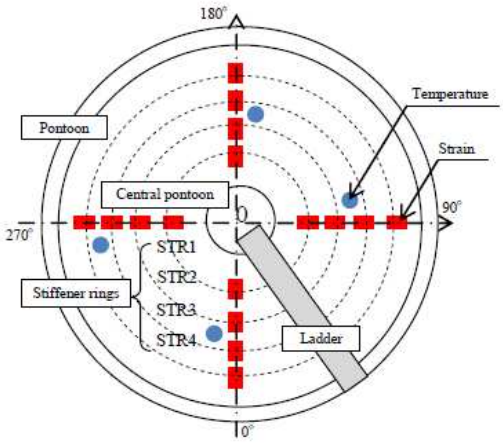

Figure 2 Layout of optical fiber gauges adhered to the floating roof.

Table 1 Sensor location on the floating roof.

	Distance from the wall of the center pontoon in each direction (m)			
	0o	***90 o***	***180 o***	***270 o***
STR1	11.8	12.1	12.0	12.0
STR2	18.0	18.0	18.0	18.0
STR3	24.1	24.0	24.0	24.0
STR4	29.5	29.5	29.5	29.5

2.2 Measurement results

Figure 3 and Figure 4 show strain and temperature amplitude history in 0^o direction during the day respectively. The origin of the time in both figures means 12A.M. Figure 3 shows that 412μStrain amplitude occurred in 12 hours around at STR 1 when temperature amplitude was 56 degree Celsius. If Young's modulus is 206GPa, 83MPa stress amplitude will occur. This value is less than that of yield stress of general structure steel (245MPa) [4]. As for the result of STR4 in Fig. 3, the buckling could occur in 9 hours. This will be discussed in the section 3.3.

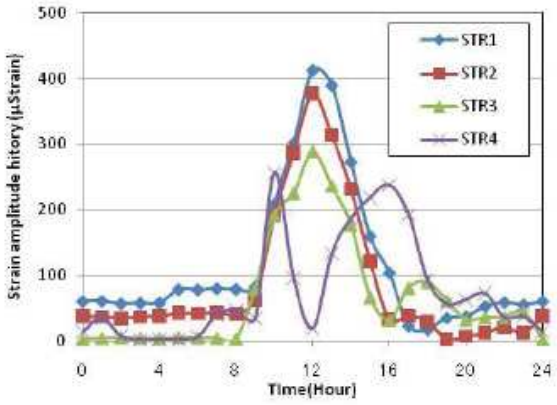

Figure 3 Strain amplitude history in 0^o direction.

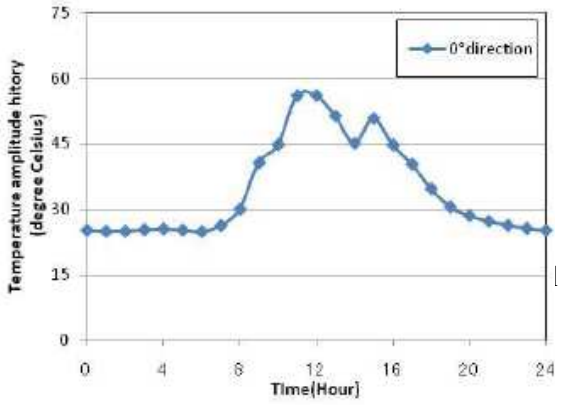

Figure 4 Temperature amplitude history in 0^o direction.

thickness of each part was equivalent to the design thickness. The number of nodes and elements was 348 and 60 respectively. Table 2 shows the material constants. The material was supposed to be the general structural steel, SS400 [4].

Figure 5 Two dimensional axial model.

Table 2 Material constants

Young's modulus	2.1×10^{11} (N/m²)
Poisson's ratio	0.3 (-)
Thermal expansion	1.13×10^{-5} (1/℃)
Thermal conductivity	51.6 (W/m℃)
Heat transfer coefficient of the wall inside the pontoon	10 (W/m²℃)
Heat transfer coefficient of the back side of the deck plate	35 (W/m²℃)

3.2 External load and constrain condition

Figure 6 shows the numerical temperature data based on measurement results and Fig. 7 shows temperature and constrain conditions. Temperature of the deck surface around the stiffener ring was around 10 degree Celsius smaller than that of other area because stiffener rings worked as a heat release fin. Even in the pontoon, the heat was likely to release from the inside wall of the pontoon. Therefore, temperature amplitude histories were given as two types of curves shown in Fig. 6. The circled numbers 1 and 2 in Fig. 7 correspond to the numbers in Fig. 6. This means that the temperature data of the circle number 1 in Fig. 6 was given to the deck surface excluding the surface above the stiffener rings. Also, the temperature data of the circle number 2 in Fig.6 was given to the pontoon surface and the surface above the stiffener rings. As for the inside wall of the pontoon shown as the line of the circle number 3 in Fig. 7, the initial temperature amplitude which was 32 degree Celsius was given. Regarding the constrain conditions, the horizontal translation was fixed on the center line and the vertical on the outer pontoon as shown in Fig. 7.

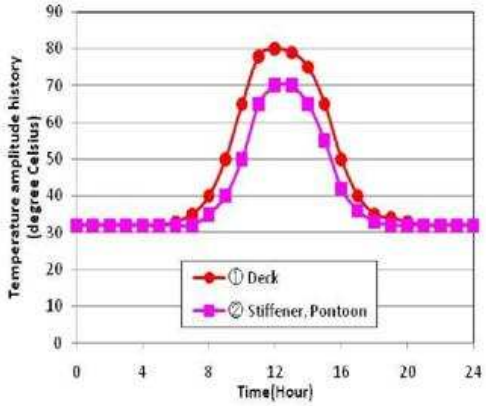

Figure 6 Numerical data of temperature amplitude history.

Figure 7 Temperature and constrain conditions on the floating roof.

3.3 Numerical results

Figure 8 shows the strain amplitude history obtained by the numerical simulation. According to Fig. 8, the strain amplitude history was subject to the temperature history and that the maximum strain amplitude occurred at around maximum temperature amplitude. Compared with Fig. 3, corresponding curves in Fig. 8 show almost the same amplitude except for STR 4. Regarding STR 4, the measurement result could show Snap-back. It is considered that imperfections in the actual floating

roof affected the deformation. The numerical model is the ideal model without imperfections, while the actual floating deck involves welded parts and additional pieces attached to the deck surface, which could be considered the origin of the buckling [5].

Figure 9 shows the effective stress history. Curves fluctuated within 8 to 18 hours. The maximum stress occurred at STR 4 in 10 hours. The maximum stress was at most 27.4MPa. In comparison with tensile strength of the general structure steel (400MPa) [4], the value of the maximum stress was fairly small. Furthermore, the maximum stress was less than the fatigue limit that is around 100MPa in the case of the general structure steel [6]. From these results, thermal stress on the floating roof was unlikely to lead to the fracture on the actual floating roof.

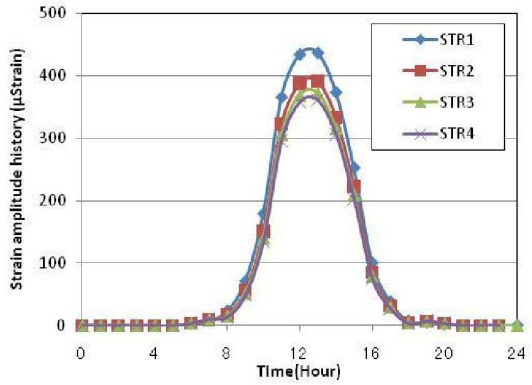

Figure 8 Strain amplitude history of the numerical simulation.

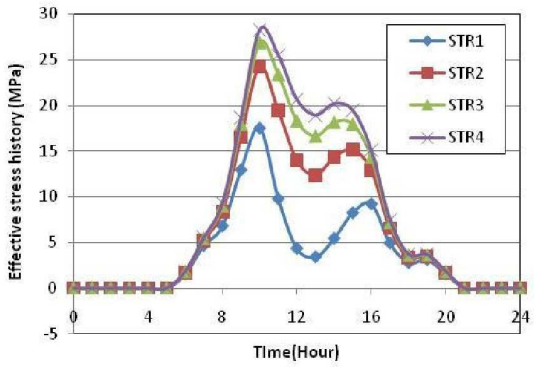

Figure 9 Effective stress amplitude history of the numerical simulation.

4. Fracture Possibility due to Thermal Stress

From the numerical results, cracks were unlikely to occur on the intact floating roof due to thermal stress. Next, initial cracks which occurred from any cause were discussed as to whether thermal stress allowed cracks to propagate or not. However, the crack occurrence involves a variety of uncertainties. Therefore, the fracture probability due to the thermal stress was estimated by using probabilistic fracture mechanics approach [7].

4.1 Fracture probability

The fracture probability P_f is shown in Eq.(1). In this study, P_f was calculated by means of Monte Carlo Method that is the way to estimate the probability of a certain event subject to the probability density function [8]. Mf and N_t describe the total number of the fracture and the event respectively. The event was randomly given according to the random function [9].

$$P_f = M_f/N_t \quad (1)$$

4.2 Flow chart to estimate fracture probability

Figure 10 shows the flow chart to estimate the fracture probability. As for an initial crack a_0, it shall be defined as a two dimensional surface crack shown in Fig. 11. The crack length a and thickness of the deck plate h have a dimension in mm. Details of the flow chart are described as follows:

1) *Initial crack*: An initial crack a_0 shall be subject to the probability density function p in Eq.(2). μ is the mean of the crack length in mm. Three cases (μ=h/3=1.6mm, h/4=1.2mm, and h/5=0.96mm) were considered. The number of the initial cracks given to the calculation was 1,000 in each case. All of the cracks were passed through the inspection process. The relatively large cracks that could be detected by the inspection were rejected and replaced. The probability function B(a), which describes that the inspection fails to detect the cracks, is given in Eq.(3) [10]. The coefficients α and β are 0.113 and 0.005 respectively.

2) *Crack propagation*: As for the crack propagation criteria, Paris law given in Eq.(4) was applied [7]. ΔK is stress intensity factor range in $MPa(m)^{1/2}$. Constant numbers C and m are 5.21×10^{-13} and 3.0 respectively [11]. The crack shall propagate in case that ΔK is larger than threshold ΔKth equal to

$2MPa(m)^{1/2}$ [11]. The stress intensity ΔK is given as difference between maximum stress intensity factor Kmax and minimum intensity factor Kmin in Eq.(5). The stress intensity factor K is determined by using the cubic stress function shown in Eq.(6) [12]. The variable ξ is shown in Fig. 12 as the ratio of the crack length a to the deck thickness h. Coefficients Ai in Eq.(6) were decided to fit the stress distribution. According to Fig. 9, maximum effective stress was 27.4MP on the deck surface attached with the stiffener ring #1. Also, the effective stress on the opposed side of the deck surface was 13.2MPa. Here, the stress function was simply defined as the linear function showing in Fig. 12. The stress intensity factor K is given as Eq.(7) based on the principle of superposition. The coefficient F0 and F1 are give as Eq.(8) and Eq.(9) according to the ratio a/t [12, 13]. Also, the periodic inspection subject to the probability function shown in Eq.(3) shall be conducted every several years. In this simulation, the four cases (no periodic inspection, every 5 years, every 8 years and every 10 years) were tested.

3) *Fracture probability*: Fracture probability was calculated by Eq.(1). The fracture condition refers to the status that the initial crack length a_0 becomes equivalent to the plate thickness h.

$$p=(1/\mu)\exp(-a_0/\mu) \quad (2)$$

$$B(a)=\beta+(1-\beta)\exp(-\alpha a) \quad (3)$$

$$da/dN=C(\Delta K)^m,\ \Delta K_{th}<\Delta K \quad (4)$$

$$\Delta K=K_{max}-K_{min} \quad (5)$$

$$\sigma(\xi) = A0+ A_1\xi + A_2\xi^2 + A_3\xi^3 \quad (6)$$

$$K=(\pi a)^{1/2}(A_0F_0+2\xi A_1F_1/\pi) \quad (7)$$

At a/t<=0.7

$$F_0=0.6820\xi^4-1.8283\xi^3+3.4051\xi^2+0.0209\xi+1.1215$$

$$F_1=1.2402\xi^4-2.2730\xi^3+2.5718\xi^2-0.0578\xi+1.0727 \quad (8)$$

At a/t>0.7

$$F_0=4729.3333-17919.6364+27100.4530-20442.3042+7692.5106-1153.4967$$

$$F_1=2688.0000-10106.3636+15174.8303-11369.3741+4250.9351-633.0513 \quad (9)$$

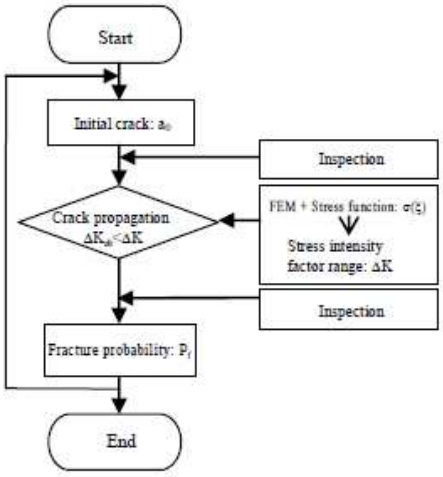

Figure 10 Flow chart for estimating fracture probability.

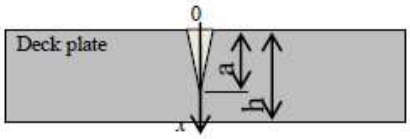

Figure 11 Two dimensional surface crack.

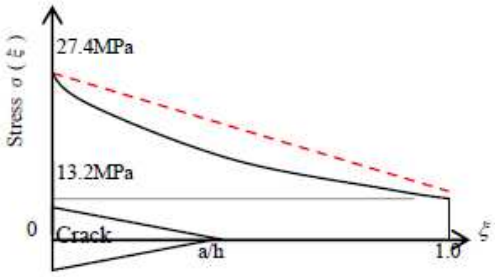

Figure 12 Coordinate system and stress function along the crack.

5. Fracture Probability Results

Figure 13 shows the fracture probability in case that average crack lengths are h/3, h/4, and h/5 without any of the initial inspection or the periodic. According to Fig. 13, the larger the average crack length is, the earlier the fracture begins to occur. In the case of h/3, the fracture begins to cause in 7.2 years and the fracture probability could attain to 0.45 in 30 years. Similarly, in the case of h/4, fracture would begin to occur in 12.8 years and the fracture probability could attain to 0.39 in 30 years. In the case of h/5, the fracture probability could attain to 0.21 within 18.8 years to 30 years.

Next, Figure 14 shows the fracture probability considering the periodic inspection (every 5, 8 and 10 years) in case of h/3. Figure 14 illustrates that the fracture probability can be approximately zero right after the periodic inspection. This result does not depend on the period of the inspection. The shorter the interval of the inspection is, the lower the maximum value of the fracture probability becomes.

The actual tank shall be inspected every 8 years. Based on the period of service (about 30 years), the fracture probability was supposed to be 4.3e-2 when the cracks on the floating roof were detected.

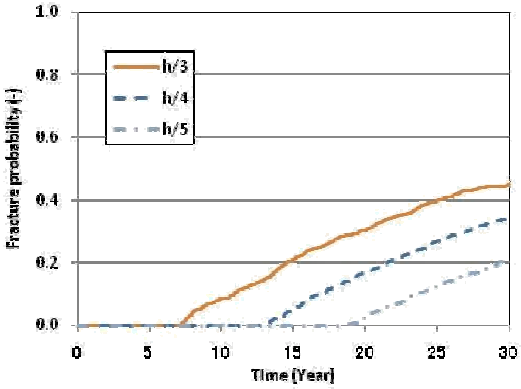

Figure 13 Fracture probability (average crack length: h/3, h/4, h/5 without any of inspections).

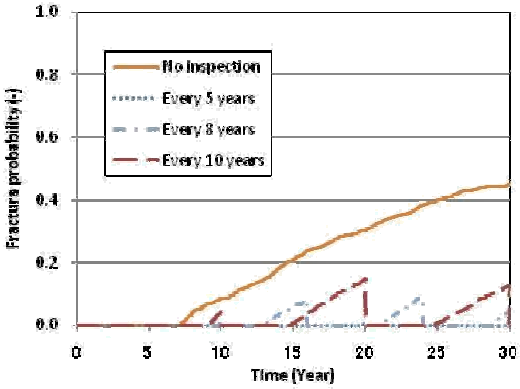

Figure 14 Fracture probability considering the periodic inspection (average crack length: h/3)

6. Conclusion

In order to investigate the cause of the crack occurrence on the floating roof, the measurement on the actual floating roof, the numerical simulation, and the fracture probabilistic estimation were carried out. Conclusions are shown as follows:

(1) Strain and temperature amplitude history on the floating roof were measured by using optical fiber gauges. The maximum strain around the stiffener rings was around 400μStrain. However, the value of the estimated maximum stress was much smaller than the value of tensile strength of the general structure steel.

(2) Thermal stress analysis was conducted by using the two dimensional axisymmetric model. Compared with the measurement results, the numerical results showed adequate value. The value of effective stress around the stiffener rings was at most 30MPa, which was less than the fatigue limit and the tensile strength of the general structure steel.

(3) The initial cracks which occurred from any cause were discussed by probabilistic fracture mechanics approach. It is considered that the initial crack could propagate and penetrate by cyclic thermal stress over time, while the cracks unlikely occur on the intact deck due to thermal stress.

(4) Considering the case in this study, the fracture probability can be estimated to be 4.3e-2. Generally, this probability would be small, while the results depend on the probability function. Therefore, other factors such as Typhoon should be also discussed in the future.

References

[1] Bob Long and Bob Gardner, "Guide to Storage Tanks and Equipment", *Wiley*, 2004: 155-156.

[2] Ken Hatayama, Shinsaku Zama, Haruki Nishi, Minoru Yamada, Yoshihiro Hirokawa, and Ryosuke Inoue, "Long-period Strong Ground Motion and Damage to Oil Storage Tanks due to the 2003 Tokachi-oki Earthquake (in Japanese)", *Journal of the Seismological Society of Japan. Second Series*, 2004; 57(2): 83-103.

[3] Minoru Yamada, Haruki Nishi, Yoshihiro Hirokawa, Shinsaku Zama, and Ken Hatayama, "On Results of Strain Measurement on the Floating Roof by Using Optical Fiber Gauge (in Japanese)", *Proc. of the 21st High Pressure Institute Conference, Tokyo, Japan*, 2009.

[4] Japanese Industrial Standards, "JIS G3101-2004 Rolled steels for general structure (in Japanese)", 2004.

[5] Bruno A. Boley, Jerome Harris Weiner, "Theory of thermal stresses", *Dover Publications, New edition*, 1997: 432-435.

[6] Ralph I. Stephens, Ali Fatemi, Robert R. Stephens, and Henry O. Fuchs, "Metal Fatigue in Engineering 2nd edition", *Wiley-Interscience*, 2000: 347-348.

[7] Motoki Yagawa, "Fracture Mechanics(in Japanese)", *Baifukan*, 1988: 116-121, 201-226.

[8] T. L. Anderson, "Fracture Mechanics", *Fundamentals and Applications 3rd editon"*, *Crc Pr I Llc*, 2005: 432-433.

[9] The Mothworks, Inc., "MATLAB help desk": http://www.mathworks.com/.

[10] U. K. Nuclear Regulatory Commission, "Reactor Safety Study", *WASH-1400, NUREG 75/014*, 1975.

[11] American Petroleum Institute, "API 579-1/ASME FFS-1 Fitness-For-Service, 2nd Edition", 2007.

[12] Japan Atomic Energy Agency, "JAERI-DATA/CODE 2001-011 (in Japanese)", 2001: 131-142.

[13] C. B. Buchalet and W. H. Bamford, "Stress Intensity Factor Solution for Continuous Surface Flaws in Reactor Pressure Vessels", *Mechanics of Crack Growth, ASTM STP 590*, 1976: 385-402.